*Int. J. Electrochem. Sci.*, 17 **(2022)** Article Number: 220965, doi: 10.20964/2022.09.61

International Journal of
ELECTROCHEMICAL
SCIENCE
www.electrochemsci.org

# Promoting Effect of Cobblestone-shaped CuI Nanoparticles Immobilized on the Copper Foil Surface on the Electrochemical Performance of the Conventional Graphite Electrode

*Keqiang Ding*[1,3*], *Fujuan Shi*[1], *Zhiheng Zhang*[2], *Boxia Li*[1], *Mengyao Di*[1] , *Mengying Yan*[1], *Lin Xu*[1], *Xueying Wang*[1], *Hui Wang*[3]

[1] Hebei Key Laboratory of Inorganic Nano-materials, Hebei Key Laboratory of Organic Functional Molecules, College of Chemistry and Materials Science, Hebei Normal University, Shijiazhuang, 050024, China
[2]Baoding Electronic Education and Equipment Technology Center, Baoding, 071000, China
[3] Hebei LingDian New Energy Technology Co., Ltd, Tangshan, 064200, China
[*]E-mail: dkeqiang@263.net

*Received:* 2 June 2022 / *Accepted:* 16 July 2022 / *Published:* 7 August 2022

It was found for the first time that cobblestone-shaped CuI nanoparticles could be facilely prepared onto the commercial copper (Cu) foil surface (denoted as CuI/Cu) via a room temperature dipping method in which the dipping solution only contained $H_2SO_4$, $CuSO_4$ and a very little amount of [Bmim]I, generating a novel chemical reaction, namely, $Cu^{2+}$+ $I^-$+ Cu (s)→CuI(s). In this work, CuI/Cu prepared in the presence of 0.3 g, 0.5 g and 1.0 g of [Bmim]I were categorized as foil a, b and c, respectively. To one's surprise, when being utilized as the current collector of the conventional graphite electrode, all as-synthesized foils exhibited a prominent positive effect on the battery performance of the conventional graphite electrode. For example, the starting discharge capacity (DC) of the graphite electrode prepared with foil b (electrode b) at 0.1 A $g^{-1}$ was as high as 688 mAh $g^{-1}$, almost 2.1 times larger than that of graphite electrode assembled using the conventional bare Cu foil (323 mAh $g^{-1}$). Especially, even at 1.0 A $g^{-1}$ after 100 cycles, the DC values of electrode b (184mAh $g^{-1}$) was still about 5.7 times that of the traditional graphite electrode (32 mAh $g^{-1}$). Developing a novel method to prepare cobblestone-shaped CuI nanoparticles and creating a new approach to greatly promote the battery performance of the conventional graphite electrode were the main contributions of this preliminary work, which was very beneficial not only to the development of CuI based nanoscience since no energy consumption was required in the preparation process of CuI nanoparticles, but also to the amelioration of the conventional graphite electrode since no variation of the electrode preparation procedure was demanded.

**Keywords:** CuI; [Bmim]I; graphite electrode; battery performance; lithium ion batteries.

## 1. INTRODUCTION

CuI is an important chemical reagent which has been applied in a wide range of application domains. On the basis of the literature survey, being employed as an optical material was indicated to be one main application of CuI in the photochemical field. For example, Fang's group [1] prepared a $Sn^{4+}$-doped CuI film through a facile solution process, and reported that the photo-detecting performance of $Sn^{4+}$-CuI/ZnO was significantly superior to that of ZnO film. Also, Zhang's group [2] systematically studied the properties of CuI nanoparticles (NPs)-based polymer solar cells (PSCs), and pointed out that CuI NPs were a kind of novel promising hole transporting material for highly efficient and stable PSCs. Yang's research team [3] thoroughly studied the transport properties of polycrystalline CuI thin films, and concluded that the hole mobility of all studied CuI thin films was about 10 $cm^2\ V^{-1}\ s^{-1}$. Kim's group [4] prepared a high-performance thin-film transistor (TFTs) and announced that the CuI:Zn semiconductors had a great application in the field of next-generation TFTs. Karuppuchamy's group [5] systematically studied the properties of an inverted perovskite solar cell assembled by a bilayer CuI@CuSCN thin film, and drew a conclusion that the power conversion efficiency of above solar cell was enhanced by about 7.6% as compared to the case of using CuI/CuSCN composites. Besides above mentioned applications, being used as catalysts in the organic chemistry field was regarded as another major utilization of CuI. In 2014, Fu's team [6] developed a new kind of organic reaction, namely, a photo-induced, copper-catalyzed monoalkylation of primary amides where CuI was creatively employed as an inexpensive catalyst. In addition, Ghosh's group [7] invented an efficient palladium-free Stille cross-coupling reaction in which allylic bromides and functionalized organostannylfuran were utilized as the starting materials and CuI was optimized as the best catalyst of this newly developed coupling reaction. Also, Liu's and his collaborators [8] prepared N-aryl DPPs via an Ullmann reaction of between H-DPPs and diaryliodonium salts where CuI, tert-butyl bipyridine and DMF were respectively employed as the catalyst, ligand and solvent. In brief, CuI is a vital chemical substance which is very crucial to the development of both photochemistry and organic chemistry. However, as far as we know, no work reporting the modification of CuI nanoparticles on the copper foil surface so as to greatly enhance the battery performance of a conventional graphite electrode was published so far.

To further improve the physicochemical properties of CuI as well as to broaden its application scopes, many novel strategies for preparing CuI have been urgently proposed in recent years. For example, Wei's group [9] succeeded in growing large-area p-type conductive CuI films onto the surface of copper films where the growth of CuI thin films was conducted by a two-step process, namely, the deposition process of copper films on glass was followed by an immersion process of copper film in the ethanol solution of iodine. Of late, an innovative layer-by-layer procedure for preparing CuI films was developed by Zhu's group [10]. In Zhu's work [10], Cu thin films were firstly deposited on quartz substrates via a radio-frequency magnetron sputtering method, and then, the resultant Cu thin films were immediately turned into CuI films upon contacting with the vapor-phase iodine. In 2020, Taunk's group [11] prepared CuI nanocrystals via a one-pot sonochemical method at room temperature in which $CuCl_2$ and KI were employed as the starting materials, and in Taunk's work [11], the influence of surfactant kinds on the structural and luminescence properties of the as-

prepared CuI nanocrystals was thoroughly investigated. Very recently, Huang's research team [12] successfully prepared size-tunable CuI tetrahedral particles using a traditional chemical redox method in which the starting materials mainly contained $CuCl_2$, AA (ascorbic acid), KI and SDS (sodium dodecyl sulfate). Although many novel approaches have been proposed to fabricate CuI particles, to the best of our knowledge, up to now, there were few reports regarding the preparation of cobblestone-shaped CuI nanoparticles onto the copper foil surface via a dipping method at room temperature.

As is known to all, copper, mainly due to its high thermal and electrical conductivities, better ductility and non-toxicity as well, is regarded as one of the most widely used metal materials in our daily production and life. Thus, copper surface modification has become a hot topic in the copper-related research areas. For example, in 2021, Fu's group [13] prepared an ultrathin surface coordination layer on a copper surface through a sodium formate present solvothermal method generating a high oxidation resistance in the air conditions, which was thought to be very beneficial to further expand the industrial application of copper. Also, as everyone knows, being employed as the current collector of an anode material was the main application of copper foil in the research field of lithium ions batteries (LIBs). Lately, modification of copper foil has been demonstrated to be a feasible way to greatly increase the electrochemical performance of an anode electrode. For example, Li's group [14] respectively prepared PEDOT and PANi onto the Cu foil surfaces forming two kinds of conductive polymer coated copper foils, and then, they came to a conclusion that Cu-graphite/Li half cells assembled with newly prepared copper foils delivered superior electrochemical performance as compared to the pristine Cu-graphite/Li half-cells. Zhu's group [15] skillfully deposited molybdenum disulfide onto a copper foil surface via a magnetron sputtering approach generating a new current collector of Cu-$MoS_2$, and they found that even after being cycled at 1 $A^{-1}$ for 300 cycles, the capacity of Cu-$MoS_2$-LTO ($Li_4Ti_5O_{12}$ was abbreviated as LTO) cell (373.9 mAh $g^{-1}$) was still significantly higher than that of the conventional Cu-LTO cell (114.94 mAh $g^{-1}$). Wen's group [16] deliberately prepared graphene-graphite coating onto the surface of a copper foil via a painting method so as to generate a novel interface between the active materials and the copper foil, and they declared that the LTO electrode assembled using the newly prepared current collector exhibited a discharge specific capacity of 167.73 mAh $g^{-1}$ at 10 C even after 2000 cycles, which showed significantly increased battery performance when compared to the LTO electrode assembled with the conventional copper foil. Although, as mentioned above, several materials have been purposely immobilized onto the conventional copper foil surface to greatly improve the electrochemical performance of the anode electrode studied, the research work describing the preparation of CuI onto the copper foil surface so as to dramatically enhance the battery performance of the commercial graphite electrode has not yet been published so far, to our knowledge. Also, the application of CuI as an electrode material of a battery was rarely reported in the past few decades. In 2021, Hao's research group [17] creatively assembled a Zn/CuI battery via which the electrode reaction of CuI was comprehensively studied, and in Hao's work, a CuI involved charge-discharge process, namely, $2CuI+Zn^{2+}+2e \leftrightarrow ZnI_2+2Cu$, was proposed for the first time. Besides Hao's work [17], as far as we know, no research works reporting the application of CuI in the battery field were published till present.

In this work, firstly, three kinds of dipping solutions were carefully prepared using $CuSO_4$, $H_2SO_4$ and [Bmim]I (1-butyl-3-methyl-imidazole iodized salt). And then, a well cleaned and dried Cu

foil was dipped in one kind of above dipping solutions for 20 min to prepare the CuI modified Cu foil (denoted as CuI/Cu). Interestingly, after the dipping process, some cobblestone-shaped nanoparticles, as revealed by SEM images, appeared on the copper foil surface. Further, it was indicated by XRD and XPS measurements that all as-prepared cobblestone-shaped nanoparticles were CuI nanoparticles. Unexpectedly, when being utilized as the current collectors of the commercial graphite electrode, all newly prepared foils, namely, foils of CuI/Cu, showed a significant positive effect on the battery performance of the graphite electrode. In particular, even at 1.0 A $g^{-1}$ after 100 cycles, the discharge capacity of the graphite electrode prepared with foil b (184 mAh $g^{-1}$) was still about 5.7 times higher than that of the conventional graphite electrode assembled using the conventional copper foil (32 mAh $g^{-1}$). Presenting a fact that CuI nanoparticles can be prepared spontaneously onto the Cu foil surface at room temperature and showing the result that using the as-prepared CuI/Cu as the current collectors of the graphite electrode was a feasible way to dramatically boost the electrochemical performance of the graphite electrode were thought as the main two merits of this work. It was worth emphasizing that no energy consumption was required in preparing nanoparticles of CuI and no variation of the preparation process was needed in assembling the graphite electrode, which was very meaningful to the large-scale industrial production of graphite electrode based LIBs.

## 2. EXPERIMENTAL DETAILS

### *2.1 Reagents and materials*

All chemical reagents such as $CuSO_4 \cdot 5H_2O$ and $H_2SO_4$ were purchased from Tianjin Reagent Company, and [Bmim]I, namely, 1-butyl-3-methyl-imidazole iodized salt, was bought from Shenyang Saiden Ionic Liquids Co., Ltd (China). The commercial copper foil and the commercial graphite powder were gratuitously provided by Hebei LingDian New Energy Technology Co., Ltd (Hebei Tangshan, China). All materials used for the battery performance test like the electrolyte of 1 M $LiPF_6$, metallic lithium foil, separator, acetylene black and PVDF (polyvinylidene fluoride) were purchased from Tianjin Lianghuo S&T Developing Co. Ltd (China). All aqueous solutions were carefully prepared using secondary distilled water.

### *2.2 Characterization*

The chemical components and the crystalline phases of the substances peeled off from the as-prepared foil surfaces were mainly characterized by using X-ray diffraction (XRD) (Bruker AXS, D8 ADVANCE, Germany). The surface morphologies of all studied foils as well as the particle sizes of the prepared cobblestone-shaped nanoparticles were examined by using scanning electron microscopy (HITACHI, SEM S-570). The element kinds as well as the approximate element contents of the substances peeled off from the studied foil surfaces were analyzed by using energy dispersive spectrometer (EDS, INCA Energy 350, England). X-ray photoelectron spectroscopy (XPS, Kratos Analytical spectrometer, Al Kα radiation) was also employed to identify the element valences of the substances peeled off from the studied foil surfaces.

*2.3 Preparation of CuI nanoparticles onto the copper foil surface at room temperature*

Firstly, a 100 mL solution containing 0.8 M $H_2SO_4$ and 0.8 M $CuSO_4$ was prepared carefully using secondary distilled water. And then, 0.3 g of [Bmim]I was discreetly added dropwise into above resultant solution under stirring to yield the final dipping solution. The dipping solutions prepared in the presence of 0.3 g, 0.5 g and 1.0 g of [Bmim]I were classified as solution A, B and C, respectively. Meanwhile, a commercial copper foil was successively washed by secondary distilled water and ethanol solution to produce a well cleaned Cu foil, and then the well cleaned Cu foil was dried in air at room temperature for 4 h to produce a well cleaned and dried Cu foil. The as-obtained Cu foil was named as foil o. Subsequently, foil o was carefully dipped in dipping solution A for 20 min to prepare the final CuI modified Cu foil (denoted as CuI/Cu). The samples of CuI/Cu produced in dipping solution A, B and C were, respectively, nominated as foil a, b and c. Correspondingly, the substances peeled off from the surfaces of foil a, b and c were, respectively, called as sample a, b and c.

*2.4 Preparation of the as-prepared foils supported graphite electrode*

Being employed as the current collector of an anode material is indicated to be the main application of copper foil in the field of LIBs [18, 19]. Although many novel anode materials have been developed in recent years, graphite powder, to our knowledge, was still the main anode material of the commercial LIBs. Thus, all as-synthesized foils were used as the current collectors of the commercial graphite electrode so as to investigate the influence of the newly prepared foils on the battery performances of the commercial graphite electrode. Generally speaking, the commercial graphite electrode was prepared based on the following steps. Firstly, the commercial graphite powder, acetylene black and PVDF (polyvinylidene fluoride) were mixed together at the mass ratio of 8:1:1 to produce a mixture, and then, a few drops of NMP (N-methylpyrrolidone) were added dropwise into above resultant mixture under vigorous stirring to yield a mud-like paste. Afterwards, the as-obtained paste was promptly painted on the surface of one as-prepared foil to generate a wet graphite electrode. Next, the resultant graphite electrode was dried under vacuum condition at 120 ºC for 6 h so as to remove the organic solvent as much as possible yielding a well-dried graphite electrode. Approximately, the loaded amount of the commercial graphite powder on each as-assembled graphite electrode was 1.5 mg per square centimeter. The graphite electrodes assembled using foil o, a, b and c were, respectively, cataloged as electrode o, a, b and c.

The two-electrode cell, also called as a half-cell, used for examining the electrochemical performance of the graphite powder, was constructed by one as-prepared electrode and a pure metallic lithium foil, which was assembled in a $N_2$ filled glove box (ZKX, Nanjing NanDa Instrument Plant, China). In the two-electrode cell, lithium foil, organic electrolyte, separator, organic electrolyte and one as-prepared electrode were sequentially pressed together forming a so-called half-cell. Here, the organic electrolyte and separator were, respectively, 1 M $LiPF_6$ and Celgard 2400. And the solvent for dissolving $LiPF_6$ was a mixed solvent which mainly contained ethyl methyl carbonate (EMC), ethylene carbonate (EC), dimethyl carbonate (DMC) and vinylene carbonate (VC). Apparently, in the resultant half-cell, the metallic lithium foil was employed as both the negative electrode and the reference

electrode. That is, the potential values appearing in this work were the potential intervals between the electrode potential of the as-prepared electrode and that of the pure metallic lithium foil. The charge/discharge equipment with a model of CT-3008W-5V20mA-S4 (Shenzhen Neware Electronics Co., Ltd. China) was used to accomplish the galvanostatic charge/discharge experiments in which the potential range was from 0.01 V to 3 V and the applied current densities were, respectively, 0.1, 0.3, 0.5 and 1.0 A $g^{-1}$.

The conventional electrochemical techniques used for analyzing the charge and discharge mechanism of an electrode material such as CV (cyclic voltammetry) and EIS (electrochemical impedance spectroscopy) were all carried out on an electrochemical workstation (EW) (CHI 660E, Shanghai Chenhua Apparatus, China) in which the green clip of the EW was connected to the as-prepared electrode and other two clips (the red clip and white clip of EW) were linked together to the metallic lithium foil. And in the EIS test, the frequency range of the alternating current (AC) was from 0.1 Hz to 100 kHz.

## 3. RESULTS AND DISCUSSION

### *3.1 Characterization of all prepared samples*

The surface morphologies of all studied foils were observed by using SEM and the SEM images with a scale of 2 μm are given in figure A of Fig.1.

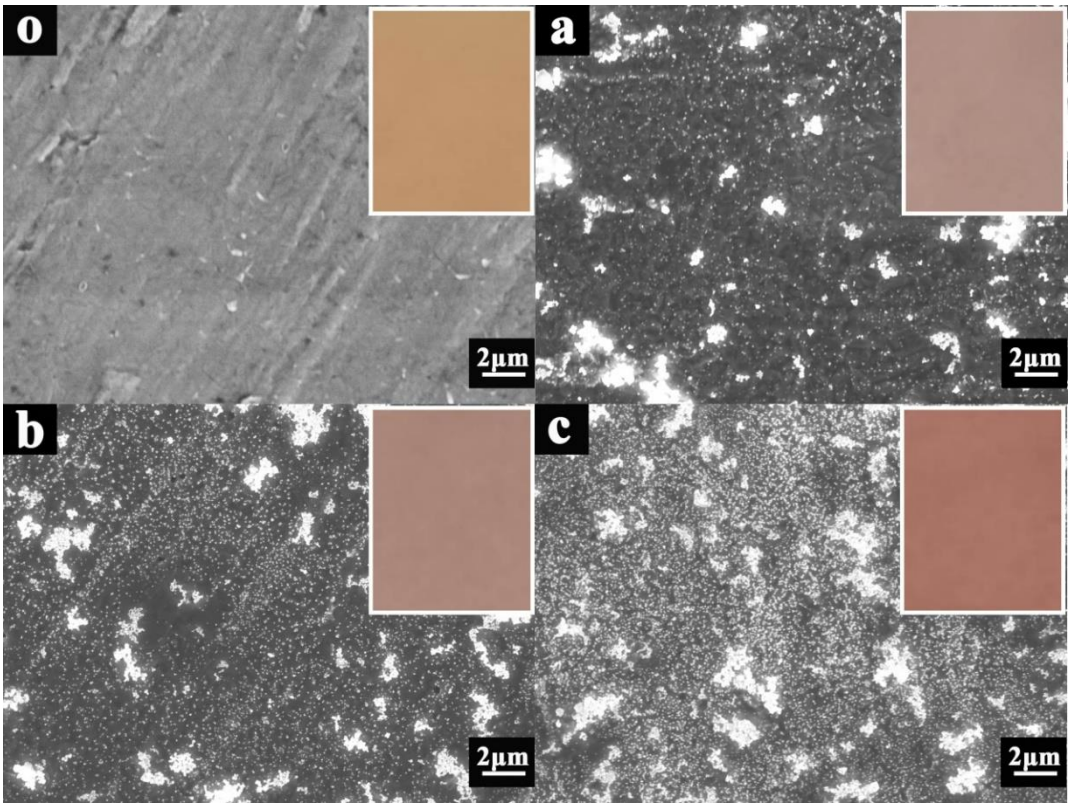


**A**

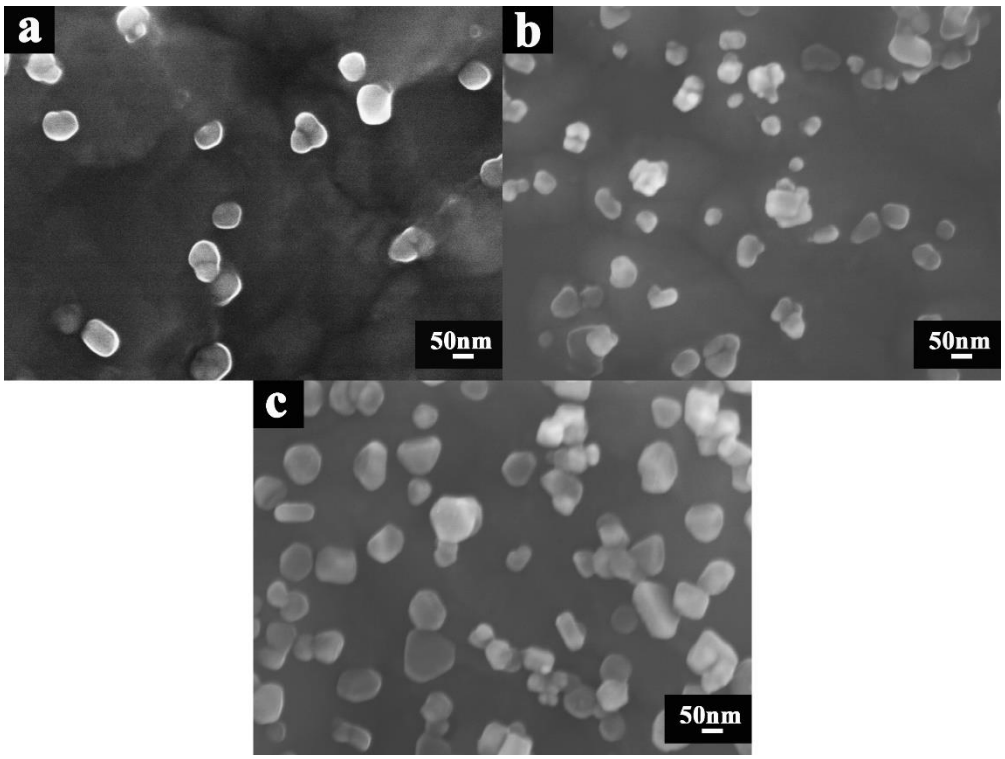


**Figure 1. (A)** SEM images with a scale of 2 μm for all studied foils. Image o was the surface SEM image of the commercial Cu foil. Image a, b and c corresponded to the surface SEM images of the as-synthesized foil a, b and c, respectively. And the photo at the upper right corner of each image was the photo of the foil studied. **(B)** SEM images with a scale of 50 nm for all as-prepared foils. Image a, b and c corresponded to the surface SEM images of foil a, b and c, respectively.

For foil o (image o), namely, the pure copper foil, some gray white streaks were clearly displayed on the pure copper foil surface which strongly indicated that no evident substances existed on the surface of the commercial copper foil. While, after the dipping treatment, as shown by image a, b and c, some white and small dots emerged distinctly on the prepared foil surfaces which substantially demonstrated that some novel materials were prepared after the dipping process. For foil a, besides some huge irregular and white plaques, some very smaller white dots were scattered on the foil surface. In the case of foil b, more amounts of very small and white particles densely immobilized on the foil surface were presented clearly, which effectively implied that the amount of small and white particles increased remarkably with increasing the content of [Bmim]I in the dipping solution. For foil c, as compared to the case of foil b, more amounts of smaller white particles appeared, which further indicated that the content of [Bmim]I in the dipping solution was a key factor in determining the amount of particles prepared. Also, as shown by the photos in each image, foil o, a, b and c delivered a pure coppery, dark brown, light brown and reddish brown color, respectively. The difference in color also indicated that the amount of the prepared particles on each foil surface was rather different from each other. SEM images with a scale of 50 nm for the surface morphologies of all newly prepared foils are provided in figure B of Fig.1. For foil a (image a), only several small particles were seen in the selected observation window, and the diameter of these prepared cobblestone-shaped particles was

close to 60 nm, which definitely indicated that all the small particles existing on the surface of foil a were nanoparticles. Apparently, for foil b, more amounts of nanoparticles appeared on its foil surface which could only be attributed to the increased concentration of [Bmim]I. Also, some small particles with a size close to 40 nm were exhibited clearly on the surface of foil b. In the case of foil c, as compared to the cases of foil a and b, more amounts of nanoparticles appeared on its surface. Apparently, the size of the particles immobilized on foil c was evidently larger than that of the particles anchored on foil a or foil b. Obviously, all as-prepared nanoparticles showed a cobblestone-shaped morphology. Although CuI particles with various morphologies such as the triangular shape [20] and the spherical shape [21] have been successfully prepared in the former works, to our knowledge, the preparation of CuI nanoparticles with a well-defined cobblestone-shaped morphology was rarely reported till present.

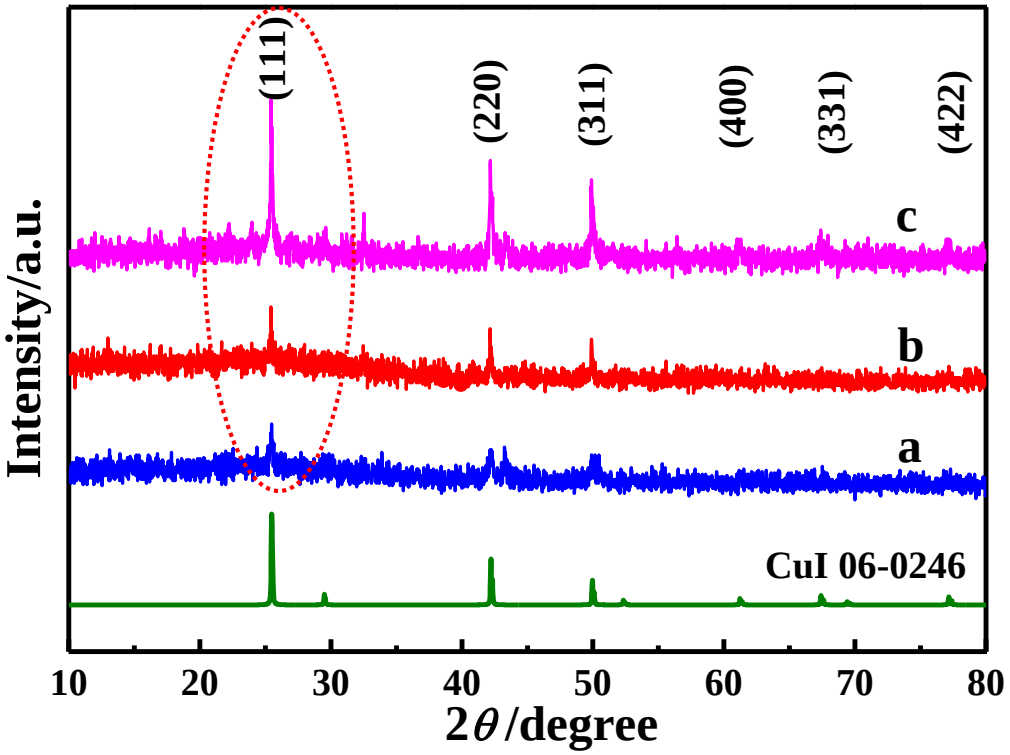


**Figure 2a.** XRD patterns for the surface substances peeled off from the as-prepared foils in which the standard XRD pattern of CuI was also presented. Pattern a, b and c corresponded to the substances obtained from foil a, b and c, respectively.

XRD patterns, including the standard XRD pattern of CuI, of the substances peeled off from the surfaces of all prepared foils are illustrated in Fig.2a. Apparently, in each XRD pattern, three evident diffraction peaks successively positioned at about 25.5°, 42.2° and 50.0° were respectively well assigned to the reflection plane of (111), (220) and (311) of cubic cuprous iodide (JCPDS, No. 06-0246) [1, 3], which strongly authenticated the successful preparation of CuI. Particularly, for foil c, other three characteristic XRD diffraction peaks belonging to CuI, namely, the diffraction peaks centered at 61.2° (400) , 67.4° (331) and 77.2° (422) [22], were also distinctly exhibited further

confirming the formation of CuI on the foil surface after the very simple dipping process. As shown by the red circled part, the diffraction peak intensity of pattern c was greatly higher that of pattern a and b, which strongly documented that the crystallinity of the substance obtained from foil c was superior to that of the substances peeled off from foil a and b. That is to say, the content of [Bmim]I in the dipping solution was also an important parameter which could directly influence the crystallinity of the as-prepared CuI nanoparticles. Summarily, XRD results shown in Fig.2a strongly demonstrated that CuI nanoparticles with a relatively higher crystallinity could be facilely prepared onto the conventional copper surface via a dipping process at room temperature. In this developed preparation process, no heating operation and no reducing agents are required, which is very meaningful to the large scale production of CuI.

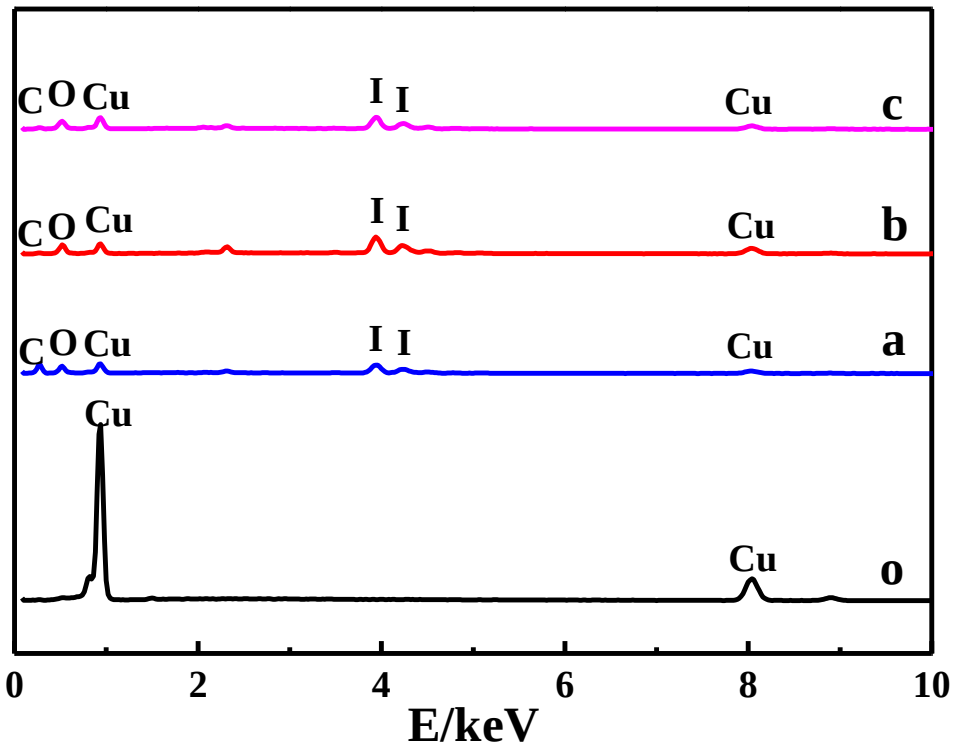


**Figure 2b.** EDS patterns for the surface substances peeled off from the studied foils. Pattern o, a, b and c corresponded to the substances scraped from foil o, a, b and c, respectively.

EDS spectra of the surface substances peeled off from foil o, a, b and c are displayed in Fig.2b. For foil o, only two peaks belonging to Cu element were exhibited implying that no evident contaminants or impurities were present in the commercial copper foil. While for other three prepared foils, except for the peaks assigned to Cu element, two small peaks indexed as the element of I were exhibited explicitly. And, the atomic contents of Cu and I elements were measured to be 12.4% and 8.8%, 27.3% and 28.2%, 28.5% and 20.3%, for the substance acquired from foil a, b and c, respectively, corresponding to an Cu to I atomic ratio of 1.4, 0.97 and 1.40. Thus, the atomic ratios of Cu to I for foil a, b and c were all greatly higher than 0.5 which effectively indicated that the substance scraped from the prepared foil surfaces should be CuI rather than $CuI_2$, being well consistent with the

XRD results (Fig.2a). Except for the element of Cu and I, the element of C and O were also detected showing atomic contents of C and O as 57.7% and 21.2%, 10.9% and 33.6%, 20.2% and 31.1%, respectively, for the substances scraped from foil a, b and c.

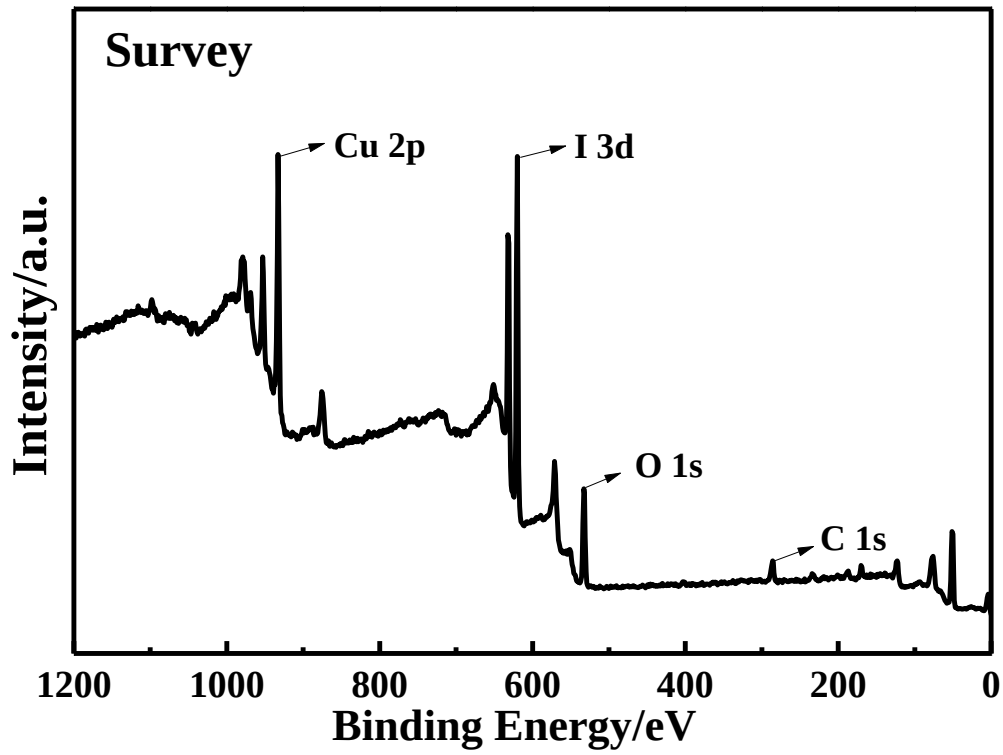


A

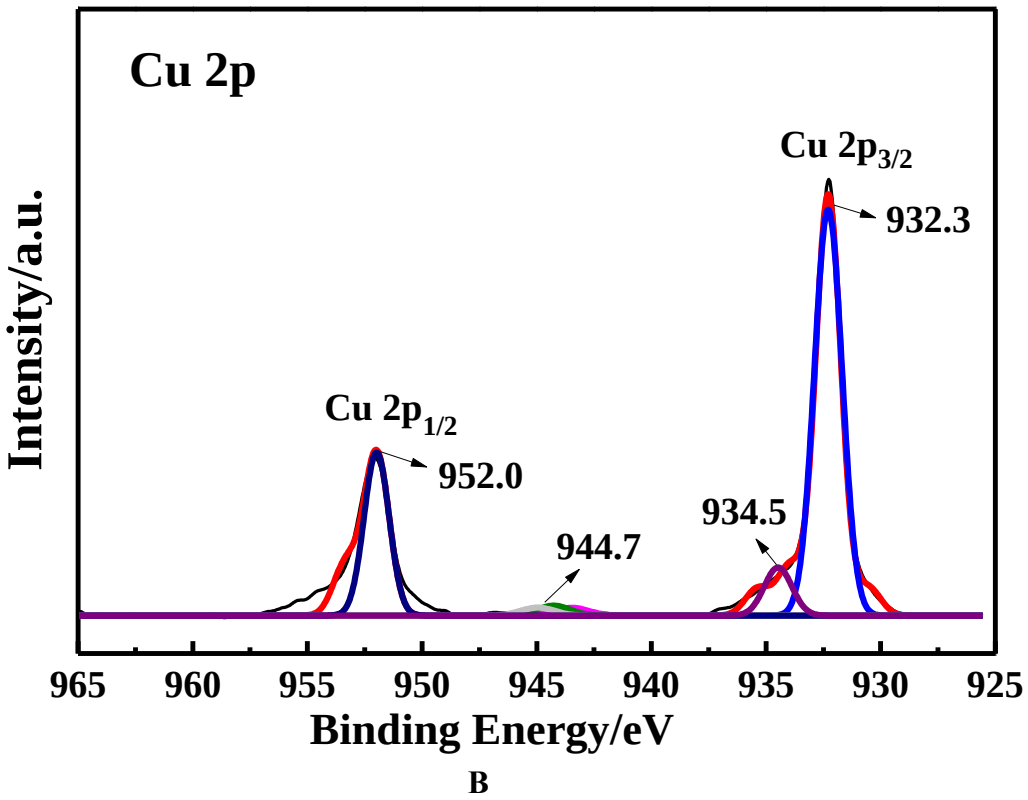


B

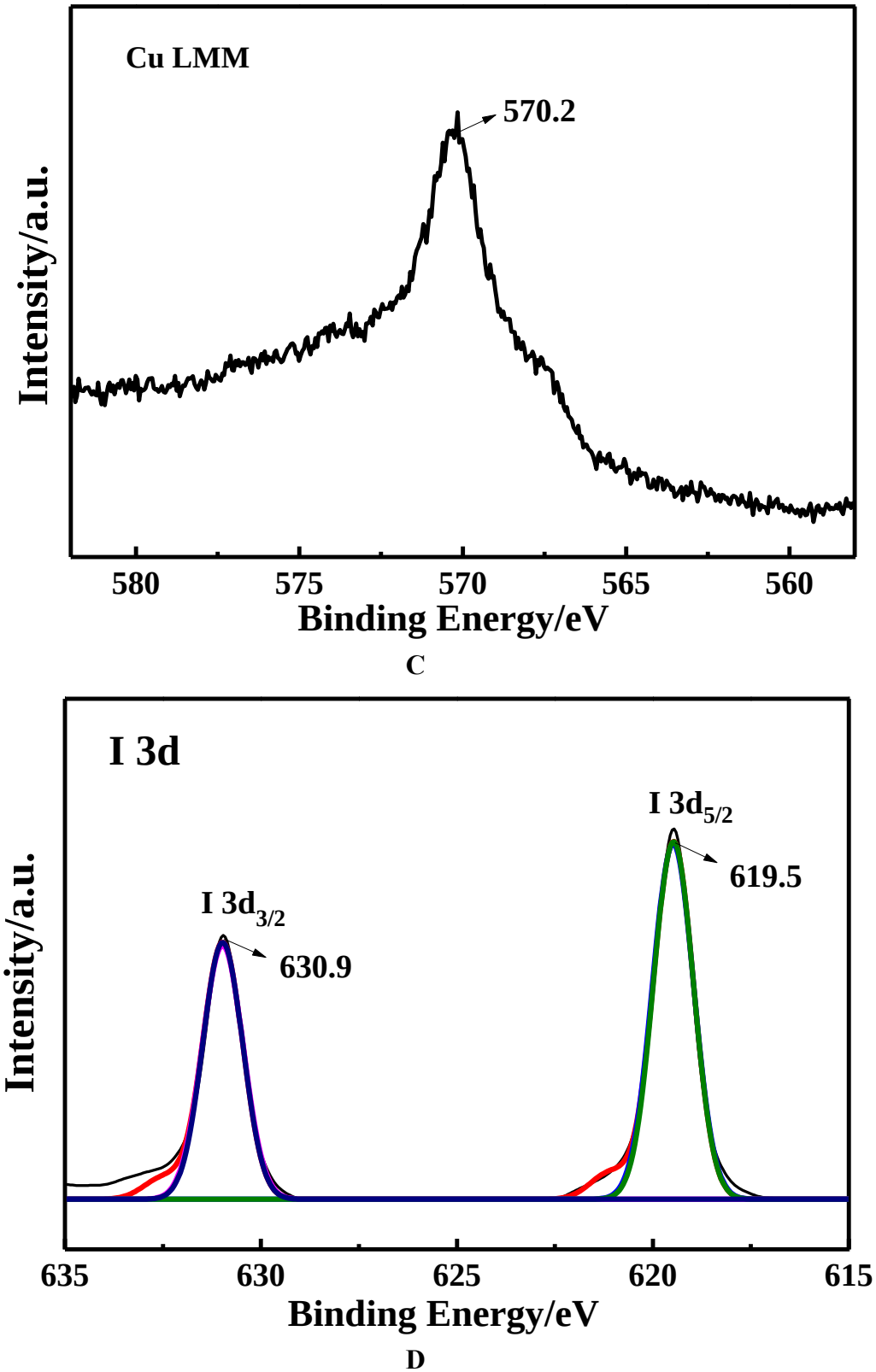


**Figure 2c.** XPS spectra of the substance scraped from the surface of foil b. (A) Wide scan XPS survey spectra. (B) XPS spectra of Cu 2p. (C) LMM spectra of Cu, (D) XPS spectra of I 3d.

Apparently, the presence of element C should be originated from the residual of [Bmim]I or

should be due to the adsorbed $CO_2$, and the existence of element O was probably ascribed to the adsorbed $CO_2$ or owing to the formation of very small amount of copper oxides on the foil surface when being exposed to the air.

To further confirm the chemical components of the new substances scraped from the foil surfaces, the material peeled off from foil b surface was also analyzed using XPS and all the results are given in the figures of Fig.2c. In the wide scan XPS survey spectra (figure A of Fig.2c), the peaks assigned to Cu, I, C and O elements were all clearly exhibited which was in accordance with the EDS results (Fig.2b). Apparently, the peak intensities of both Cu and I element were all significantly higher than that of C and O element again indicating that the main substance of the materials scraped from foil b surface was CuI. In figure B of Fig.2c, two large peaks located at the binding energies (BEs) of 932.3 eV and 952.0 eV were respectively assigned to the Cu 2p core of Cu $2p_{3/2}$ and Cu $2p_{1/2}$, strongly indicating the existence of $Cu^+$ [23]. Meanwhile, two small peaks successively centered at 944.7 eV [24] and 934.5 eV [25] were, respectively, identified as the typical satellite peaks of Cu (II) $2p_{1/2}$ and Cu (II) $2p_{3/2}$ for $Cu^{2+}$, which could only be attributed to the formation of a very little amount of copper oxides in the studied sample. Evidently, the intensities of the peaks assignable to Cu (I) were remarkably higher than that of the peaks attributed to both Cu (II). It strongly demonstrated that the content of Cu(I)-containing substance was significantly higher than that of Cu(II)-containing substance, being well coincident with the XRD and EDS results. The Cu LMM spectra of the substance peeled off from foil b surface are displayed in figure C of Fig.2c. Apparently, one huge BE peak at 570.2 eV was displayed which further indicated the presence of $Cu^+$ on the basis of the previous works [25, 26, 27]. The results of XPS and LMM spectra effectively demonstrated that the existing form of Cu element in the substances peeled off from foil b surface was $Cu^+$ rather than $Cu^{2+}$ which accorded well with the analysis results of both XRD and EDS patterns. In the high resolution XPS spectra of I element (figure D of Fig.2c), two evident peaks centered at 619.5 and 630.9 eV were, respectively, attributable to the BEs of I $3d_{5/2}$ and I $3d_{3/2}$, further signifying that the element of I was present in the form of $I^-$ [28] in the studied material. Also, no other BE peaks were found in the I 3d XPS spectra which strongly confirmed that $I^-$ was the unique existing form of I element in the substances scraped from foil b surface. Therefore, along with the XRD and EDS results, it was convinced that the chemical substance used for constituting those cobblestone-shaped nanoparticles shown in Fig.1 was CuI rather than other substances. To our knowledge, this is the first time to report the preparation of cobblestone-shaped CuI nanoparticles via a dipping process at room temperature.

### *3.2 Electrochemical performances of graphite electrodes assembled using as-prepared foils*

The initial discharge capacity value of an electrode material was an important data which was closely related to its eventual rate capability and cycling performance.

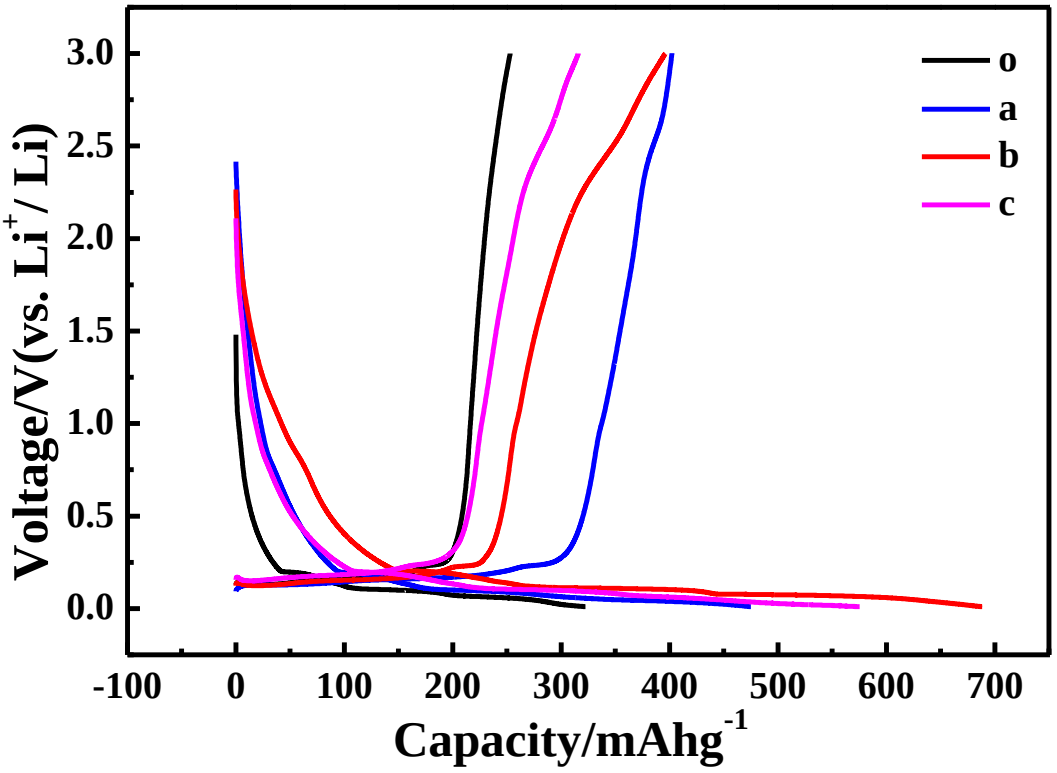


**Figure 3a.** The initial charge-discharge curves of the graphite electrode assembled using newly prepared foils which were recorded at 0.1A $g^{-1}$ within a potential range of 0.01-3.0V. Curve o, a, b and c, respectively, corresponded to electrode o, a, b and c.

The curves shown in Fig.3a are the starting charge-discharge plots of electrode o, a, b and c in which the applied current density was 0.1A $g^{-1}$ and the potential range was from 0.01 V to 3 V. Evidently, the curve shapes of electrode a, b and c were very similar to that of electrode o, signifying that graphite powder [29], rather than the newly prepared CuI nanoparticles, was the main material participating in the lithiation and delithiation process. The initial discharge capacity (DC) values of electrode o, a, b and c were detected to be 323, 475, 688 and 575 mAh $g^{-1}$, respectively. That is to say, the DC values of all the graphite electrodes constructed by using CuI coated foils were memorably higher than that of the graphite electrode prepared by using the conventional copper foil. Especially, the DC value of electrode b was almost 2.1 times larger than that of the routine graphite electrode. In other words, the immobilization of cobblestone-shaped CuI nanoparticles on the copper foil surface had significantly increased the initial DC value of the conventional graphite electrode. In addition, the initial DC values of the graphite electrodes assembled by using CuI coated foils were all remarkably larger than the theoretical DC value of 372 mAh $g^{-1}$ of a pure graphite electrode, which strongly indicated that some novel materials have been triggered to be novel lithium storage materials taking part in the charge and discharge process. Also, the potential intervals between the charge and discharge platform of electrode a, b and c were greatly lower than that of electrode o. For example, the potential interval values at 200 mAh $g^{-1}$ were estimated to be about 0.24 V, 0.16 V, 0.04 V and 0.08 V for electrode o, a, b and c, respectively. That is, as compared to the case of using the bare copper foil, the over potentials existing in the charge and discharge process were dramatically reduced through

employing the CuI modified copper foils as the current collectors of the conventional graphite electrode. Namely, the reversibility of the charge and discharge process of electrode a, b and c was superior to that of electrode o, which was very advantageous to the electrochemical performance enhancement of an electrode material [30].

The rate performances of all studied electrodes are compared in Fig.3b in which the current densities of 0.1, 0.3, 0.5 and 1.0 A $g^{-1}$ were respectively applied and in each rate test the electrode was cycled at a given current density for 10 cycles. Apparently, in each rate measurement, electrode b (as shown by the red dotted line) delivered the largest DC value among all studied electrodes, for instance, the DC value under the current density of 0.5 A $g^{-1}$ recorded at the tenth cycle for electrode o, a, b and c were, respectively, tested to be about 36.7, 78.6, 126.9 and 98.0 mAh $g^{-1}$. Particularly, even at 1.0A $g^{-1}$, the DC value measured at the tenth cycle of electrode b (52.8 mAh $g^{-1}$) was almost 3.4 times larger than that of electrode o (15.5 mAh $g^{-1}$). Interestingly, as the applied current density was adjusted again to be 0.1 A $g^{-1}$, as shown by the rightmost curves, the DC values of both electrode b and c were still remarkably higher than that of electrode o, showing a satisfied rate stability. In brief, electrode b delivered the best rate capability amongst all studied electrodes.

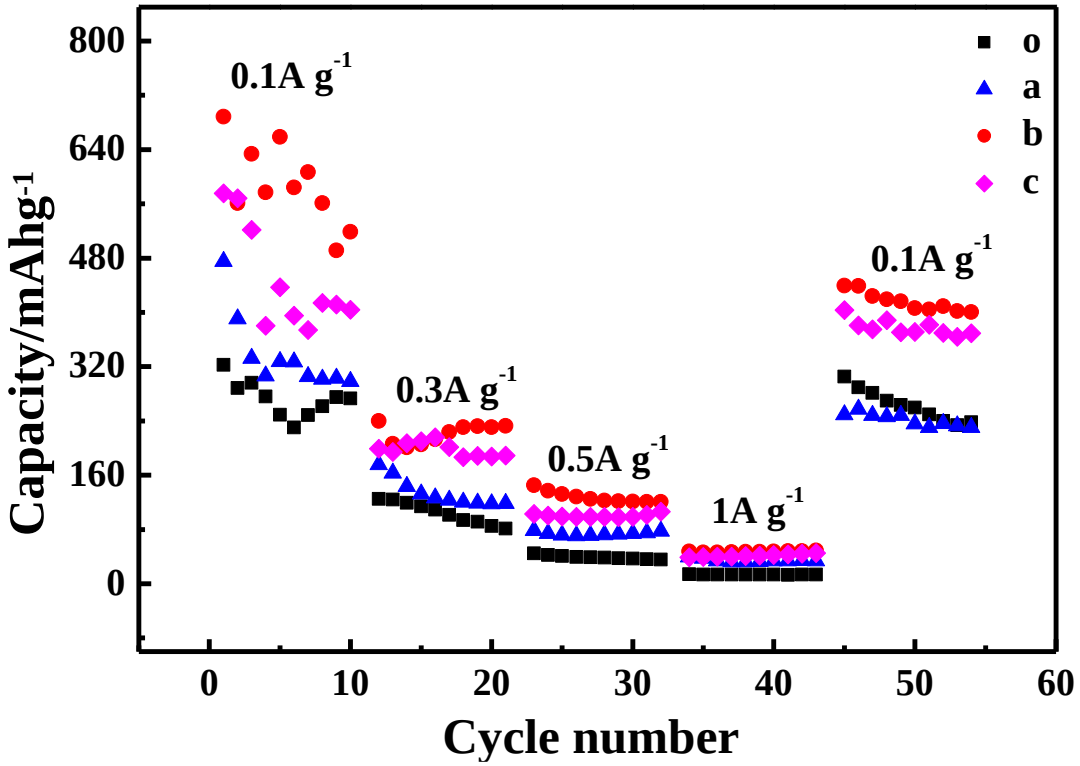


**Figure 3b.** Rate capabilities of the graphite electrode assembled using newly prepared foils in which the applied current densities were 0.1, 0.3, 0.5 and 1 A $g^{-1}$. In each rate test, the electrode was cycled for 10 cycles. Curve o, a, b and c, respectively, corresponded to electrode o, a, b and c. After the sequential rate test, the applied current density was returned to be 0.1 A $g^{-1}$, and the results are shown by the rightmost curves.

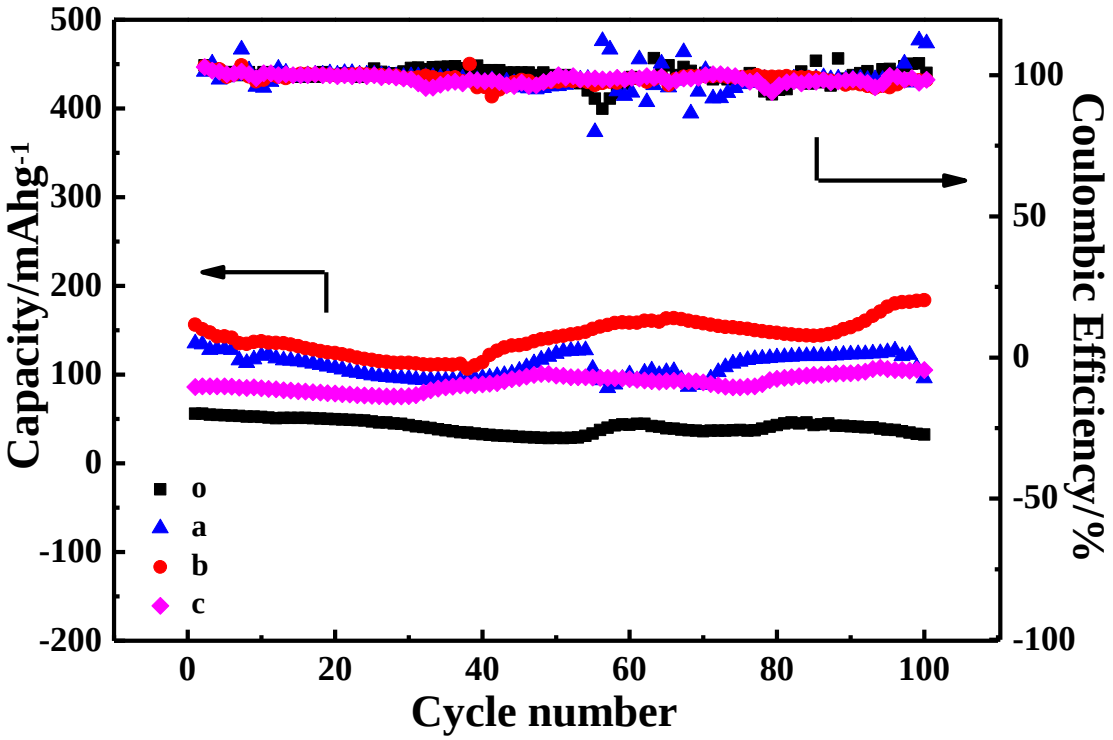


**Figure 3c.** Cycling performances of all prepared graphite electrodes, which were measured at 1 A $g^{-1}$ for 100 cycles. The upper part plots are the curves showing the relationship between the cycling number and the coulombic efficiency. Curve o, a, b and c, respectively, corresponded to electrode o, a, b and c.

The cycling behaviors of all studied electrodes are given in Fig.3c in which each electrode was cycled at 1.0 A $g^{-1}$ for 100 cycles. The upper plots in Fig. 3c were the curves showing the relationship between the cycling number and the coulombic efficiency of all studied electrodes. The DC values of electrode o, a, b and c at the $100^{th}$ cycle were recorded to be 36.7, 94.9, 184.7 and 105.8 mAh $g^{-1}$, respectively. Thus, electrode b exhibited the largest DC value among all studied electrodes though some fluctuations were also displayed in its curve. Also, the coulombic efficiencies of all studied electrode were close to 100% suggesting that no evident energy loss occurred during the charge and discharge process. Thus, the utilization of the as-prepared CuI modified copper foil as the current collector of a common graphite electrode was a feasible way not only for enhancing the DC values but also for raising the rate capability of a commercial graphite electrode.

### *3.3 Analyzing the promoting effect of the as-prepared foils on the electrochemical performance of the conventional graphite electrode*

Why the immobilization of CuI nanoparticles on the copper foil surface could greatly increase the electrochemical performance of a common graphite electrode? To explain this interesting phenomenon, the following experiments were carried out systematically.

The CV curves of all studied electrodes are illustrated in Fig.4a. For the conventional graphite

electrode (black curve), i.e., electrode o, besides an evident electro-reduction peak at about 0.01V, in the whole potential range, only one large electro-oxidation peak centered at about 0.45 V was displayed in the positive direction potential scanning, showing a very similar CV curve shape to that of the pure graphite electrode [31].

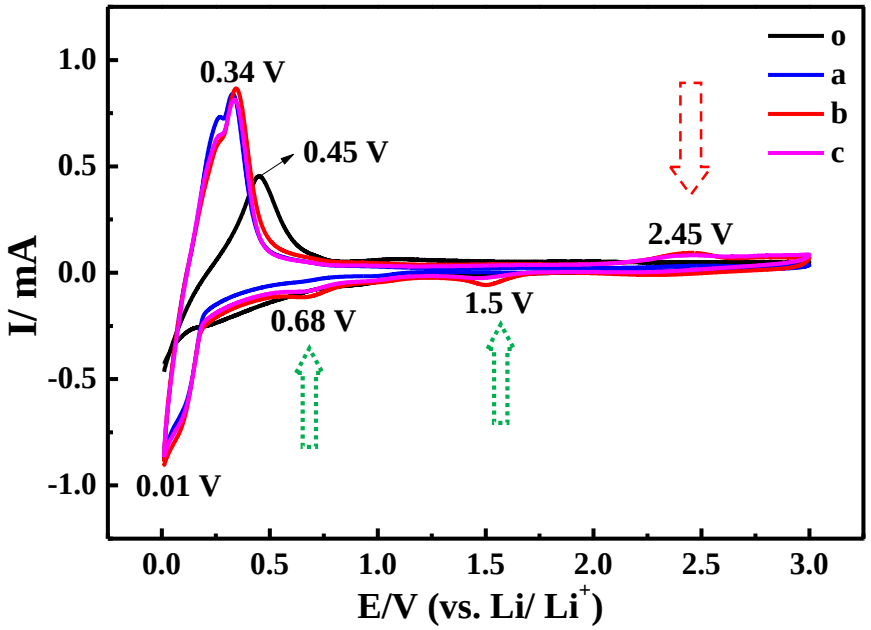


**Figure 4a.** CV curves for all studied graphite electrodes which were measured at the scan rate of 1mV $s^{-1}$. Curve o, a, b and c, respectively, corresponded to electrode o, a, b and c.

Thus, according to the previous work, the electro-oxidation peak at 0.45 V should be attributed to the deintercalation of lithium ions [31], namely, the delithiation process from the $LiC_6$ phase to the intermediates and finally to C [31]. Correspondingly, the electro-reduction peak at about 0.01V should be originated from the intercalation of lithium ions into C and the $LiC_y$ ($y \leq 6$) like intermediates [32] so as to form the final product of $LiC_6$. Interestingly, for electrode a, b and c, a huge electro-oxidation peak at around 0.34 V was exhibited clearly which should also be assigned to the deintercalation of lithium ions [31]. Thus, the over potential of the deintercalation process occurring in the graphite electrode was approximately reduced by about 110 mV through using the as-prepared CuI modified copper foil as the current collector of the common graphite electrode, which could generate a faster kinetics of lithium ion deintercalation process. Also, adjacent to the huge peak at 0.34 V, a shoulder shaped peak at 0.26V was presented distinctly which indicated that the mechanism of the lithium ion deintercalation process occurring in electrode a, b and c was slightly different from that happening in the routine graphite electrode. Noticeably, for electrode a, b and c, a small evident electro-oxidation peak also emerged at 2.45V in the positive direction potential scanning, and in the negative direction potential scanning, two evident electro-reduction peaks were successively observed at 1.50 V and 0.68V. The presence of novel CV peaks effectively demonstrated that some novel substances have been activated to take part in the charge-discharge process, showing a different lithium ions charge-discharge mechanism as compared to that of the traditional graphite electrode. Evidently, the total CV

peak areas of electrode a, b and c were drastically larger than that of electrode o, which substantially indicated that more amount of lithium ions have participated in the charge and discharge process when using CuI modified copper foils as the current collectors of the graphite electrodes. Thus, the larger CV peak area and the appearance of some novel CV peaks were thought to be the main reasons providing electrode a, b and c an improved battery performance relative to that of the traditional graphite electrode.

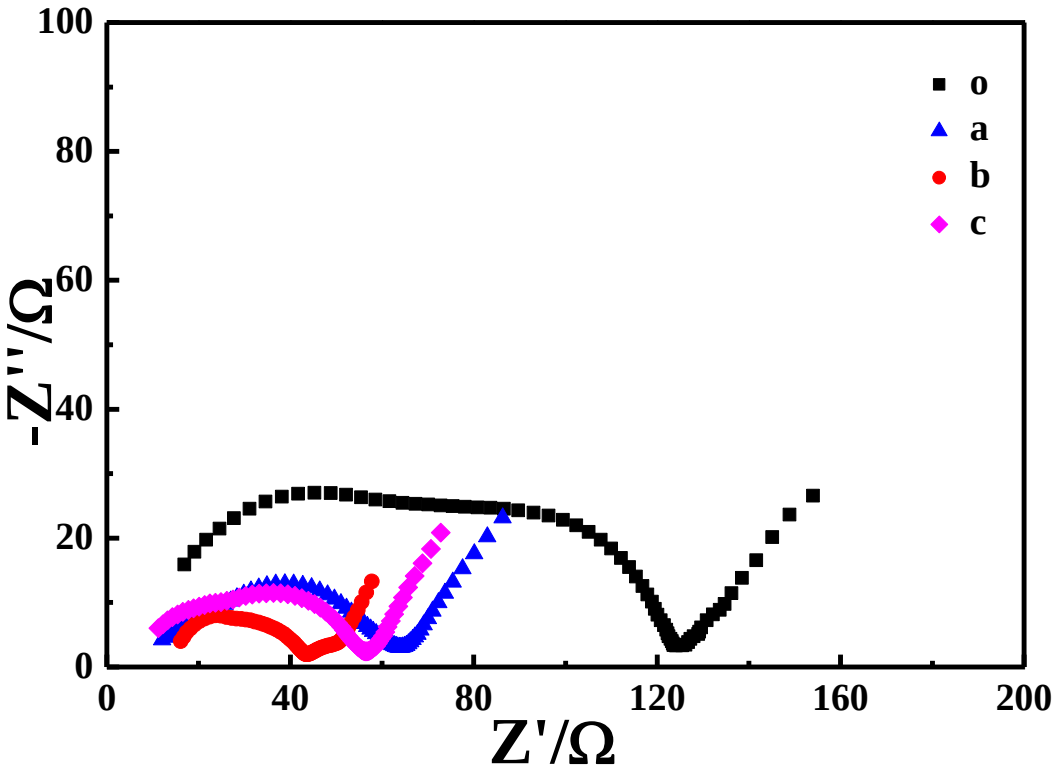


**Figure 4b.** Nyquist plots of all studied graphite electrodes which were recorded in the frequency region of 0.1-$10^5$ Hz. Curve o, a, b and c corresponded to electrode o, a, b and c, respectively.

Nyquist plots for all studied electrodes are collected in Fig.4b. For the common graphite electrode, namely, electrode o, a huge bow-shaped semicircle that was likely constructed by two semicircles was explicitly exhibited in the higher frequency region, which was followed by an oblique line in the lower frequency region. Similar curve shapes were found in Nyquist plots of electrode a, b and c suggesting that the main surface microstructures of all studied electrodes were very similar to each other [33]. Generally, the semicircle appearing in a Nyquist plot was originated from the presence of a parallel circuit consisting of a resistance element and a capacitive element [33], and the diameter of the semicircle was roughly equivalent to the charge transfer resistance value ($R_{ct}$) [34]. For simplicity, the diameter of the entire bow-shaped semicircle was approximately assumed to be the value of $R_{ct}$. Thus, the values of $R_{ct}$ for electrode o, a, b and c were roughly evaluated to be 125, 64, 44 and 56 Ω, respectively. That is, as compared to that of the conventional graphite electrode, all graphite electrodes prepared using CuI modified copper foils showed much smaller $R_{ct}$ values, generating a relatively faster kinetics.

According to the previous work [35], the lithium ion diffusion coefficient ($D_{Li^+}$) values of all studied electrodes were also roughly calculated employing the following two equations, namely,

$$Z_{re} = R_s + R_{ct} + \sigma\, \omega^{-1/2} \quad (1)$$

$$D_{Li^+} = \frac{(RT)^2}{2(An^2F^2C_{Li^+}\sigma)^2} \quad (2)$$

The scientific meanings of all parameters in equation (1) and (2) have been well described in the former work [35]. That is, the σ value was the slope of the curves showing the relationship between $Z_{re}$ ( i.e., Z') and $\omega^{-1/2}$ ($\omega=2\pi f$ ). And next, the obtained σ values were put in equation (2) to calculate the final values of $D_{Li^+}$. To make things easier, all parameters existing in equation (2), besides σ, were thought to be identical for each studied electrode. Consequently, a smaller σ value should correspond to a lager $D_{Li^+}$ value.

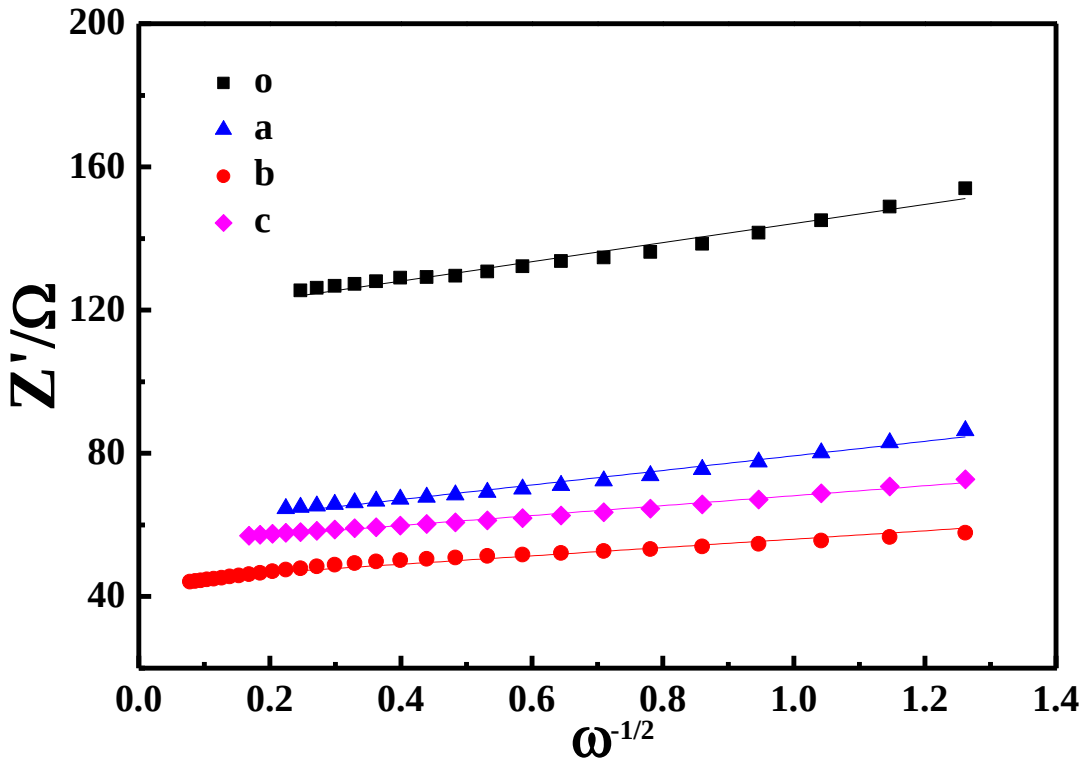


**Figure 4c.** The curves exhibiting the relationship between Z' and $\omega^{-1/2}$. It should be noted that the values of both Z' and ω were acquired from the results of Fig. 4b. Curve o, a, b and c corresponded to electrode o, a, b and c, respectively.

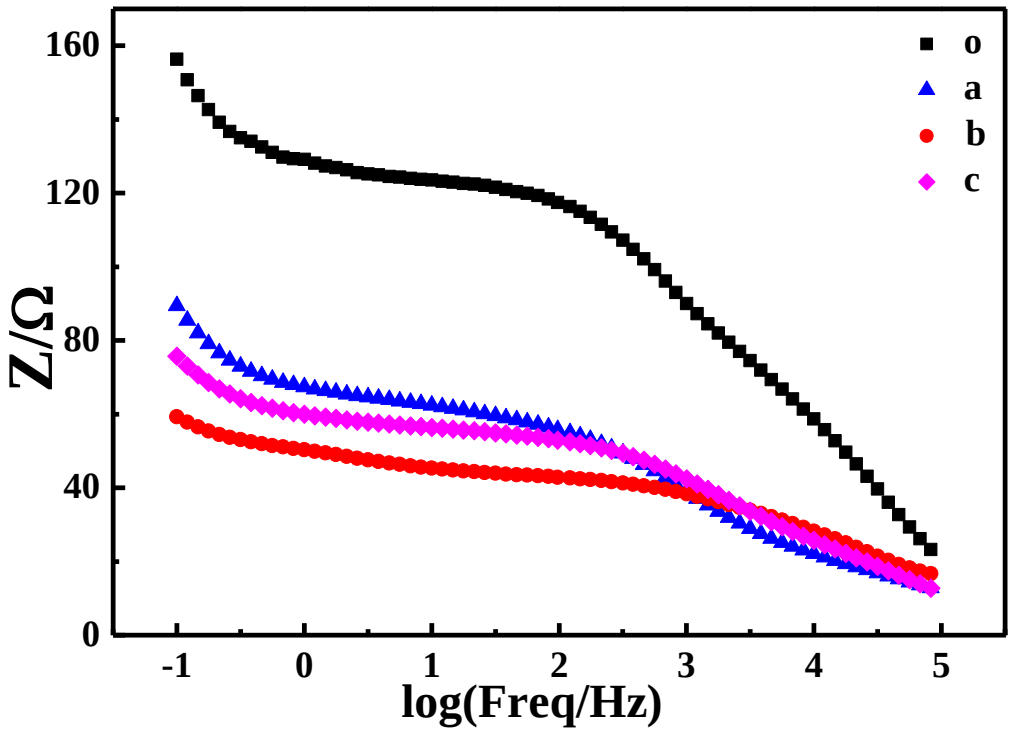


**Figure 4d.** The curves showing the relationship between the applied frequency and total resistance value of the electrodes studied. Also, the data of Fig. 4d were obtained from the results of Fig. 4b. Curve o, a, b and c corresponded to electrode o, a, b and c, respectively.

As illustrated in Fig.4c, the σ values for electrode a, b and c were evidently lower than that of electrode o. And curve b exhibited the smallest value of σ amongst all curves. Thus, electrode b, due to its minimum σ value, delivered the largest value of $D_{Li}^{+}$ among all studied electrodes. This result strongly indicated that utilizing the CuI modified copper foil as the current collector of the traditional graphite electrode was an available approach to greatly enlarge the $D_{Li}^{+}$ value. As far as we know, this interesting result has never been reported in the previous works. To further study the influence of CuI nanoparticles coated foils on the total resistance values of the studied electrodes, the curves showing the relationship between the frequency and the total resistance values are provided in Fig.4d. Obviously, in the whole measuring frequency range, electrode b showed the smallest resistance values amongst all studied electrodes. For example, at the frequency of 0.1 Hz, the total resistance values were measured to be about 157, 90, 59 and 77 Ω, respectively, for electrode o, a, b and c. Evidently, the greatly reduced total resistance values of the newly prepared electrodes should mainly be attributed to the presence of CuI nanoparticles on the copper foil surface. Probably, a novel transition interface was created between the graphite powder and copper foil when using CuI nanoparticles coated copper foil as the current collector of the graphite electrode, which was favorable to greatly reduce the internal resistance of a lithium ion battery (LIB).

The influence of the immobilized CuI nanoparticles on the surface wettability of all studied foils was further investigated through measuring the contact angles between the organic electrolyte of $LiPF_6$ and the studied copper foil surface and the results are shown in Fig.5a. The contact angle values were measured to be 34.8 °, 27.6°, 21.4° and 22.5° for foil o, a, b and c, respectively. Thus, the contact

angle values of all CuI coated copper foils were much lower than that of the pure copper foil which strongly indicated that the adhesion between the organic electrolyte of $LiFP_6$ and the current collector of copper foil was greatly ameliorated through immobilizing CuI nanoparticles onto the copper foil surface [36]. Electrode b exhibited the smallest contact angle value among all studied copper foils, showing a better wettability, which was very beneficial to the electrochemical performance improvement of an electrode.

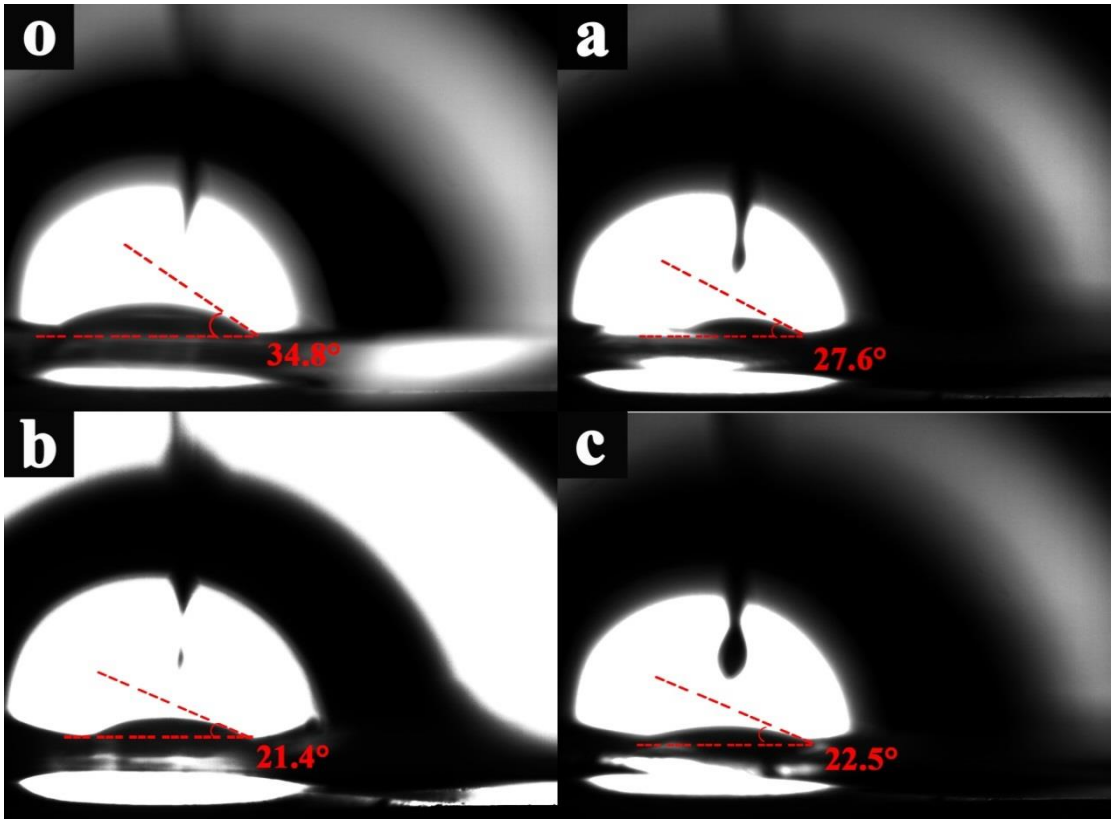


**Figure 5a.** Photos took while measuring the contact angles between 1 M $LiFP_6$ and the studied foils. Photo o, a, b and c, respectively, corresponded to the case of measuring the contact angles of foil o, a, b and c.

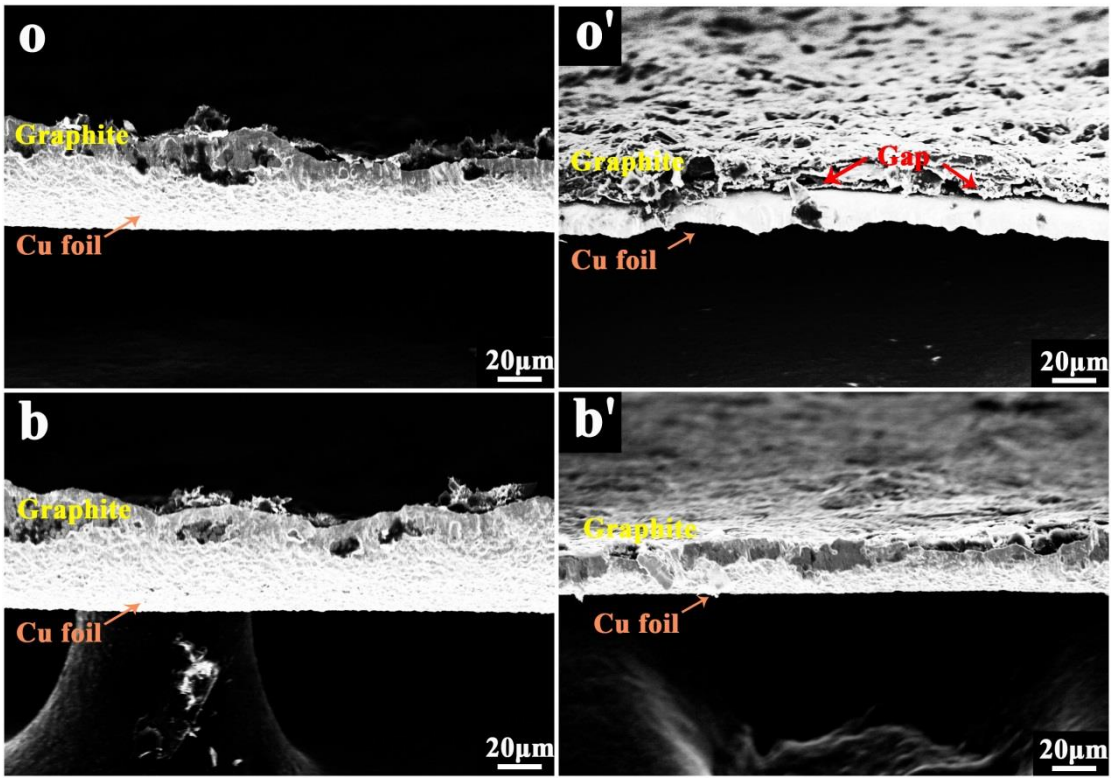


**Figure 5b.** SEM images with a scale of 20 μm of the interface cross section between the graphite powder and the current collectors before and after 100 cycles at 1 A $g^{-1}$. Image o and b corresponded to the images before 100 cycles, and image o' and b' corresponded to the images after 100 cycles. Image o and o' represented the case of using electrode o, and image b and b' represented the case of using electrode b.

To intuitively study the influence of the as-prepared copper foils on the microstructure of the interface between the graphite powder and the current collector, the SEM images of the interface between the graphite powder and the current collector before and after 100 cycles at 1.0 A $g^{-1}$ are illustrated in Fig.5b. For the conventional graphite electrode (image o and o'), as indicated by the red arrows, some evident gaps (image o') between the graphite powder and the conventional copper foil appeared after 100 cycles at 1.0 A $g^{-1}$. In contrast, for electrode b, no obvious gaps (image b') between the graphite powder and the CuI modified copper foil were found after 100 cycles at 1 A $g^{-1}$ which substantially indicated that the binding force between the graphite powder and the current collector was greatly boosted by the modification of CuI nanoparticles onto the conventional copper foil surface.

The SEM images of the current collector surface before and after 100 cycles at 1.0 A $g^{-1}$ are also given in Fig.5c. That is to say, after 100 cycles at 1 A $g^{-1}$, the half-cells were disassembled and the graphite powder was carefully scraped from the current collector surface generating a used current collector. And then, the current collector surface adjacent to the graphite powders was subjected to SEM characterization. For the conventional copper foil before the cycling measurement (image o), some scratches were displayed clearly. While, after the cycling measurement (image o'), some huge holes were exhibited distinctly effectively suggesting that the surface of the pure copper foil was violently corroded during the charge-discharge process. After 100 cycles at 1.0 A $g^{-1}$, a large number of evenly distributed small pits (image b'), rather than the huge holes, were presented on foil b surface.

Above SEM image comparison strongly indicated that the corrosion process of the copper foil during the charge-discharge process was greatly impeded by the immobilization of CuI nanoparticles on the conventional copper foil surface. The EDS patterns of the substances scrapped from the foil b surface before and after 100 cycles at 1.0 A $g^{-1}$ are displayed in Fig.5d. For the scraped substances before long cycling testing (pattern b), the peaks assigned to the element of I were distinctly exhibited. Interestingly, after the long-term cycling test, as shown by pattern b', the peaks belonging to I element totally vanished. This result strongly demonstrated that CuI has participated in the charge-discharge process or CuI has been completely consumed during the lithiation and delithiation processes, which accorded well with CV results (Fig.4a) that several novel redox peaks emerged in the CV curves when using the CuI coated copper foil as the current collector of the conventional graphite electrode.

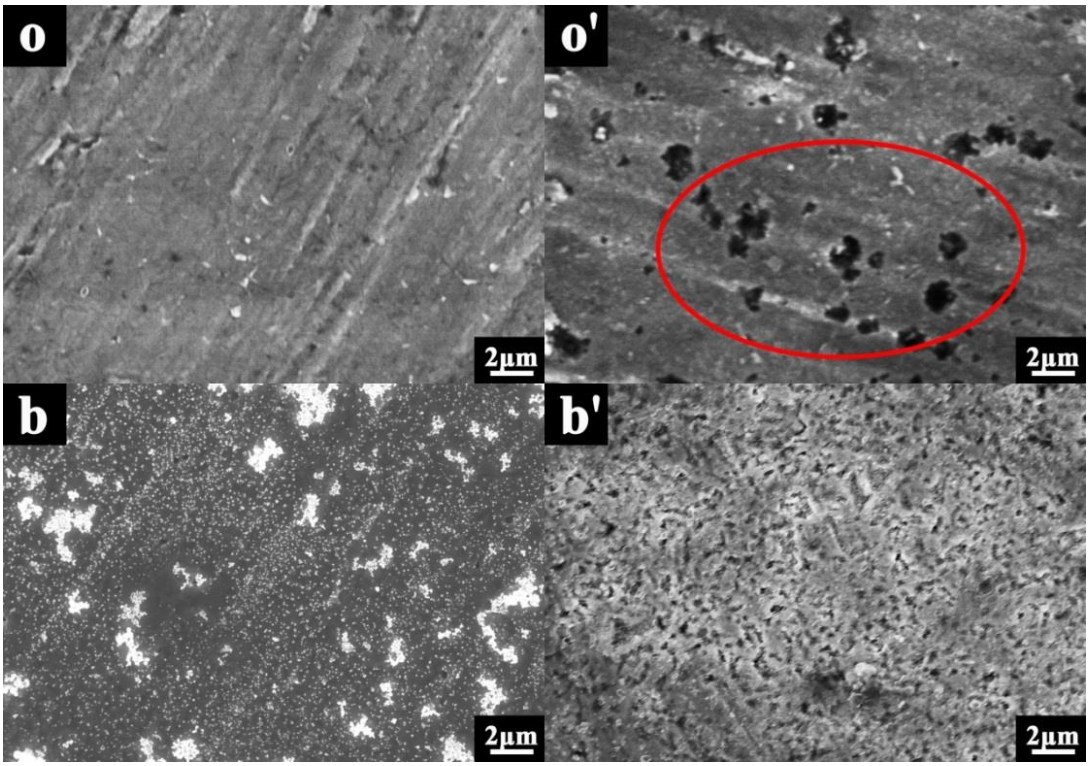


**Figure 5c.** SEM images of the foil surface next to the graphite powder before and after 100 cycles at 1 A $g^{-1}$. Image o and b corresponded to the surface SEM images before 100 cycles, and image o' and b' corresponded to the surface SEM images after 100 cycles. Image o and o' were the images of foil o, and image b and b' were the images of foil b.

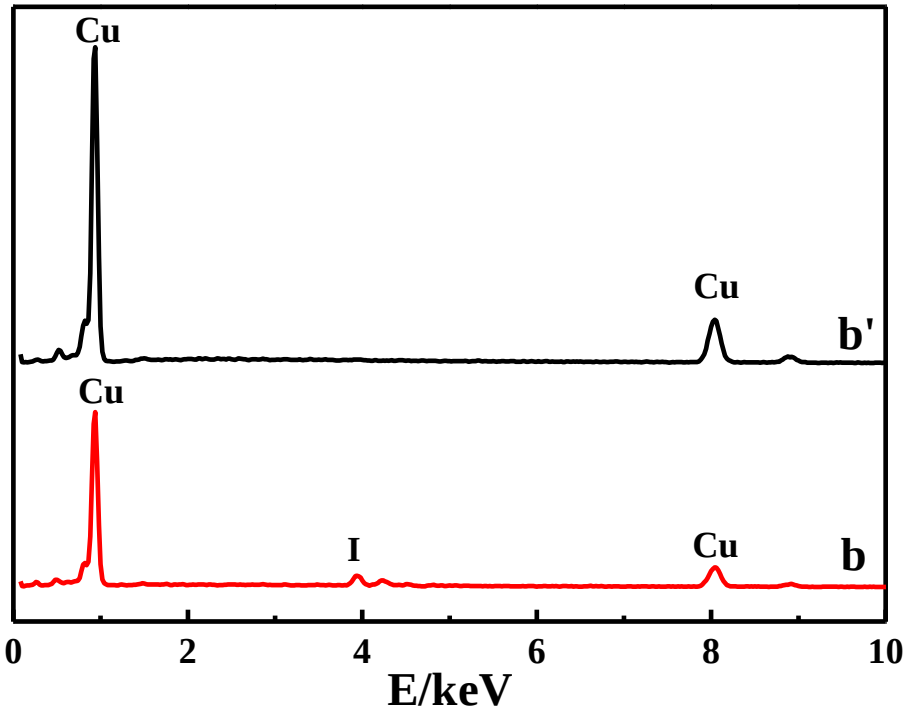


**Figure 5d.** EDS patterns for the substances scraped from the surface of foil b before and after 100 cycles at 1 A $g^{-1}$. It should be noted that the substances tested were scraped from the side of foil b adjacent to the graphite powder. Pattern b and b' respectively corresponded to the substances before and after 100 cycles at 1 A $g^{-1}$.

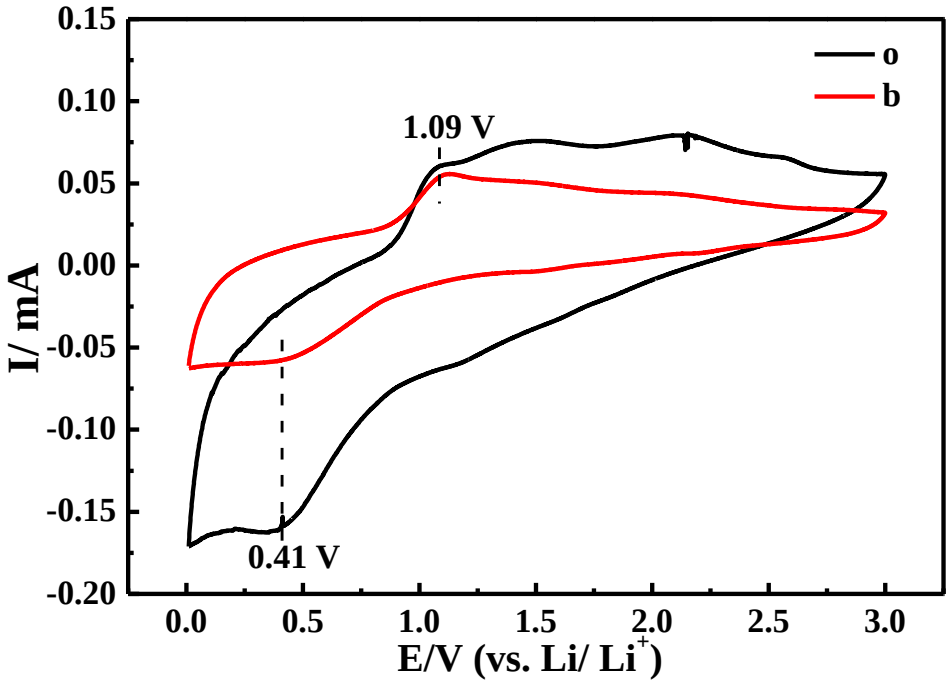


**Figure 5e.** CV curves for two-electrode cells which were measured at the scan rate of 1mV $s^{-1}$. Here, except for the absence of graphite powder, other testing conditions were all identical to that of the two-electrode cell investigated in this work. Curve o corresponded to the case of the two-electrode cell assembled by foil o and a lithium foil, and curve b corresponded to the case of the two-electrode cell assembled by foil b and a lithium foil.

To further study the influence of the as-prepared cobblestone-shaped CuI nanoparticles on the properties of the copper foil, the CV curves of both foil b and the pure copper foil (foil o) are shown in Fig.5e in which the potential scanning rate is 1 mV $s^{-1}$. It should be noted that the measurement conditions of Fig.5e were the same as that of Fig.4a except that no graphite powder was present in the as-assembled two-electrode cell. To one's surprise, as shown by the black curve, a well-defined CV curve was presented in the case of foil o. In the positive direction potential scanning, four electro-oxidation peaks located respectively at 1.09, 1.43, 2.11 and 2.55V were exhibited clearly which strongly indicated that the pure copper foil was electrochemically oxidized during the charging process. While, in the negative direction potential scanning, a huge electrochemical reduction peak was clearly displayed at around 0.41V suggesting that some copper ions released were again electrochemically reduced to be metallic copper or to be copper ions with lower chemical valences. Generally, in the case of the pure copper foil (foil o), the presence of CV curve should be attributed to the electrochemical redox of copper foil itself, or due to the electrochemical redox of the organic electrolyte. As revealed by image o' in Fig.5c, the pure copper foil surface was severely corroded during cycling, thus, the black curve shown in Fig.5e should be mainly originated from the electrochemical redox of copper foil itself. Interestingly, in the case of foil b (as shown by the red curve), one electro-oxidation peak at around 1.09 V and an electro-reduction peak at about 0.41V were clearly displayed in the whole testing potential window. In this case, those small electro-oxidation peaks appearing in the CV curves of foil o totally vanished which substantially indicated that the immobilization of CuI nanoparticles on the conventional copper foil greatly retarded the electro-oxidation process of copper foil in the organic electrolyte of 1 M $LiPF_6$. Apparently, the CV curve area for foil b was much smaller than that of foil o indicating that the corrosion process of pure copper foil was greatly inhibited by the immobilization of CuI on its surface, which was well consistent with the fact that as compared to the case of using foil o less amount of huge holes were created on the foil b surface after 100 cycles at 1.0 A $g^{-1}$ (image b and b' in Fig.5c). In short, the coating of CuI nanoparticles on the pure copper foil surface significantly improved the corrosion resistance of pure copper foil which was very profitable to long term cycling operation of a copper foil supported graphite electrode.

Summarily, some novel lithium storage substances activated by the presence of CuI nanoparticles (Fig.4a), the evidently reduced over-potential (Fig.4a), the greatly reduced $R_{ct}$ value (Fig.4b), the enlarged lithium ion diffusion coefficient (Fig.4c), the significantly reduced total resistance (Fig.4d), the remarkably increased wettability (Fig.5a) and the improved corrosion resistance (Fig.5e) were analyzed as the main reasons endowing the CuI modified copper foils a significant promoting effect on the electrochemical performance of the common graphite electrode. Particularly, electrode b, namely, the graphite electrode assembled by using foil b, exhibited a significantly increased electrochemical performance as compared to the traditional graphite electrode. In this work, no heating treatment and no strong oxidant or reducing agent were involved in preparing CuI nanoparticles, and no change of the graphite electrode preparation process was required, which were all believed to be very meaningful to the large scale production of graphite electrode based LIBs.

## 4. CONCLUSIONS

For the first time, cobblestone-shaped CuI nanoparticles (CS-CuI NPs) were prepared onto the conventional copper foil surface at room temperature via a dipping method where the dipping solution only consisted of $H_2SO_4$, $CuSO_4$ and a very little amount of [Bmim]I. Here, three kinds of CS-CuI NPs were fabricated through varying the added amount of [Bmim]I. It was revealed by SEM that the concentration of [Bmim]I was a key factor which could greatly affect both the morphology and the particle sizes of the as-synthesized particles. And, as indicated by the XRD and XPS analysis, all nanoparticles emerging on the copper foil surface after the dipping process were CuI nanoparticles. More importantly, when being utilized as the current collector of the common graphite electrode, all prepared CuI-modified copper foils exhibited an evident promoting effect on the battery performance of the conventional graphite electrode. The DC value of electrode b at $100^{th}$ cycle under the current density of 1.0A $g^{-1}$ (184.7 $mAhg^{-1}$) was about 5 times higher than that of the conventional graphite electrode (36.7 $mAhg^{-1}$ ), showing a dramatically increased battery performance. The newly created lithium storage substances, the greatly decreased $R_{ct}$ value, the enlarged higher $D_{Li^+}$ value, the significantly reduced total resistance, the remarkably increased wettability and the improved corrosion resistance were regarded as the main causes rendering foil b supported graphite electrode (electrode b ) a remarkably increased electrochemical performance. To sum up, a novel approach to prepare cobblestone-shaped CuI nanoparticles was developed in this work in which no energy consumption was required and a new feasible way to greatly enhance the battery properties of the conventional graphite electrode was also invented in this preliminary work where no variation of the graphite electrode procedure was needed.

ACKNOWLEDGEMENTS
This work was supported by the Innovation ability improvement project of Hebei province (225A4402D) and Graduate student innovation ability training program of Hebei Normal University (CXZZSS2022060)

## References

1. S. Li, Y. Zhang, W. Yang and X. Fang, *Adv. Mater. Interfaces*, 6 (2019) 1900669.
2. Y. Zhong, Y. Li, X. Lan, J. Wang, J. Wang and Y. Zhang, *IEEE J. Photovolt.*, 11 (2021) 668.
3. M. Kneiß, C. Yang, J. Barzola-Quiquia, G. Benndorf, H. von Wenckstern, P. Esquinazi, M. Lorenz and M. Grundmann, *Adv. Mater. Interfaces*, 5 (2018) 1701411.
4. A. Liu, H. Zhu, W.-T. Park, S.-J. Kim, H. Kim, M.-G. Kim and Y.-Y. Noh, *Nat. Commun.*, 11 (2020) 4309.
5. K. Ramachandran, C. Jeganathan and S. Karuppuchamy, *J. Alloys Compd.*, 881 (2021) 160530.
6. 6.H.-Q. Do, S. Bachman, A. Bissember, J. Peters and G. Fu, *J. Am. Chem. Soc.*, 136 (2014) 2162.
7. A. Ghosh, J. Born, A. Veitschegger and M. Jurica, *J. Org. Chem.*, 85 (2020) 8111.
8. W. Jiang, Z. Liu, D. Zhu, W. Zheng, L. Chen, X. Zhang, G. Zhang, Y. Yi, L. Jiang and D. Zhang, *Angew. Chem., Int. Ed.*, 60 (2021) 10700.
9. M. Wang, H. Wei, Y. Wu, C. Yang, P. Han, F. Juan, Y. Chen, F. Xu and B. Cao, *Phys. B*, 573 (2019) 45.

10. F. Geng, L. Yang, B. Dai, S. Guo, G. Gao, L. Xu, J. Han, A. Bolshakov and J. Zhu, *Surf. Coat. Technol.*, 361 (2019) 396.
11. N. Singh and M. Taunk, *ChemistrySelect*, 5 (2020) 12236.
12. C.-H. Chang, M. Madasu, M.-H. Wu, P.-L. Hsieh and M. Huang, *J. Colloid Interface Sci.*, 591 (2021) 1.
13. J. Peng, B. Chen, Z. Wang, J. Guo, B. Wu, S. Hao, Q. Zhang, L. Gu, Q. Zhou, Z. Liu, S. Hong, S. You, A. Fu, Z. Shi, H. Xie, D. Cao, C.-J. Lin, G. Fu, L.-S. Zheng, Y. Jiang and N. Zheng, *Nature*, 586 (2020) 390.
14. S. Wen, Z. Li, C. Zou, W. Zhong, C. Wang, J. Chen and S. Zhong, *New J. Chem.*, 45 (2021) 10541.
15. X. Zhu, X. Jiang, X. Yao, Y. Leng, L. Wang and Q. Xue, *ACS Appl. Mater. Interfaces*, 11 (2019) 26880.
16. W. Qin, H. Liu, J. An and X. Wen, *J. Power Sources*, 479 (2020) 229090.
17. J. Hao, L. Yuan, B. Johannessen, Y. Zhu, Y. Jiao, C. Ye, F. Xie and S.-Z. Qiao, *Angew. Chem., Int. Ed.*, 60 (2021) 25114.
18. S. Sun, D. He, P. Li, Y. Liu, Q. Wan, Q. Tan, Z. Liu, F. An, G. Gong and X. Qu, *J. Power Sources*, 454 (2020) 227907.
19. K. Ding, J. Han, X. Gao, L. Zhou and R. Qu, *Mater. Chem. Phys.*, 232 (2019) 354.
20. F. Geng, L. Yang, B. Dai, S. Guo, G. Gao, L. Xu, J. Han, A. Bolshakov and J. Zhu, *Surf. Coat. Technol.*, 360 (2019) 269.
21. E. Vance, C. Grant, I. Karatchevtseva, Z. Aly, A. Stopic, J. Harrison, G. Thorogood, H. Wong and D. Gregg, *J. Nucl. Mater.*, 505 (2018) 143.
22. S. Uthayaraj, D. Karunarathne, G. Kumara, T. Murugathas, S. Rasalingam, R. Rajapakse, P. Ravirajan and D. Velauthapillai, *Materials*, 12 (2019) 2037.
23. M. Kumar, V. Bhatt, O. Nayal, S. Sharma, V. Kumar, M. Thakur, N. Kumar, R. Bal, B. Singh and U. Sharma, *Catal. Sci. Technol.*, 7 (2017) 2857.
24. L. Fang, S. Dong, L. Shi and Q. Sun, *New J. Chem.*, 43 (2019) 12744.
25. P. Liu and E. Hensen, *J. Am. Chem. Soc.*, 135 (2013) 14032.
26. T. Wang, J. Wang and Y. Wu, *Corros. Sci.*, 97 (2015) 89.
27. C. Xue, W. Hao, W. Cheng, J. Ma and R. Li, *Chem. Eng. J.*, 375 (2019) 12204.
28. A. Liu, H. Zhu, W.-T. Park, S.-J. Kang, Y. Xu, M.-G. Kim and Y.-Y. Noh, *Adv. Mater.*, 30 (2018) 1802379.
29. Z. Ma, Y. Zhuang, Y. Deng, X. Song, X. Zuo, X. Xiao and J. Nan, *J. Power Sources*, 376 (2018) 91.
30. K. Ding, T. Okajima and T. Ohsaka, *Electrochemistry*, 75 (2007) 35.
31. L. Yang, W. Guo, Y. Shi and Y. Wu, *J. Alloys Compd.*, 501 (2010) 218.
32. J. Xu, X. Wang, N. Yuan, B. Hu, J. Ding and S. Ge, *J. Power Sources*, 430 (2019) 74.
33. K. Ding, H. Gu, C. Zheng, L. Liu, L. Liu, X. Yan and Z. Guo, *Electrochim. Acta*, 146 (2014) 585.
34. K. Ding, J. Zhao, Y. Sun, Y. Chen, B. Wei, Y. Zhang and J. Pan, *Ceram. Int.*, 42 (2016) 19187.
35. T.-F. Yi, H. Liu, Y.-R. Zhu, L.-J. Jiang, Y. Xie and R.-S. Zhu, *J. Power Sources*, 215 (2012) 258.
36. K. Peta, T. Bartkowiak, P. Galek and M. Mendak, *Tribol. Int.*, 163 (2021) 107139.